IMPROVING PERFORMANCE OF POLYMER FIBER REINFORCED SANDWICH X-JOINTS IN NAVAL VESSELS – PART I: DESIGN ASPECTS

Christian Berggreen*, Christian Lundsgaard-Larsen*, Kasper Karlsen*, Claus Jenstrup* and Brian Hayman**
***Department of Mechanical Engineering, Technical University of Denmark**
****Det Norske Veritas and University of Oslo, Norway**

Keywords: *Sandwich, X-joint, debond, fiber bridging, core inserts*

Abstract

In many naval ships of fiber composite sandwich construction an X-joint exists where the end bulkhead of the superstructure is attached to the deck, with a bulkhead placed in the same vertical plane below the deck. As the hull girder flexes this joint is subjected to alternating tensile and compressive loading in the vertical direction. The paper aims to provide an improved basis for the design of such X-joints, focusing on the prevention of crushing of the core under compressive load. Strain distributions are investigated by both laboratory tests and numerical modeling, and design criteria for core inserts are presented. The tensile loading case is addressed in a companion paper.

1 Introduction

Sandwich construction with face laminates of fibre reinforced plastics has been used in a number of naval ships where low weight has been an important factor. In most cases the superstructure does not cover the full length of the hull, and in some cases it also does not cover the full width. In such an arrangement, the end bulkhead of the superstructure is usually attached to the deck in a position lined up with a transverse bulkhead placed underneath the deck. This results in an X-joint configuration with the deck running continuously through the joint and the bulkheads connected to its face laminates, see Fig. 1.

As the hull girder flexes due to motion of the ship in waves, compressive and tensile vertical loadings are exerted alternately on such an X-joint. The compressive loading may lead to crushing of the sandwich core within the deck as it passes through the joint, while the tensile loading tends to pull the upper face laminate off the deck. It is important to prevent these modes of failure through good detailing of the joint.

A literature search has revealed an appreciable amount of research into the behavior and optimization of sandwich T-joints [2-4], but very little information about X-joints. On this basis it is concluded that X-joint design has up to now been largely based on experience of testing and analysis of T-joints. As the X-joint is a “harder” detail than the T-joint, in the sense that the stresses are likely to be more concentrated and that possibilities for redistribution may be more limited, it is suggested that such a procedure may be unconservative and thereby an important cause of observed joint failures.

The work presented in this paper will deal with the design aspects of X-joints exposed to compressive loading while the damage tolerance of the joint in case of damage is covered in part II [1] of this paper. The strain distribution in two often applied X-joint designs has been investigated both numerically using a commercial FE code (ABAQUS) and experimentally using advanced digital deformation measurements. Through these analyses and a validation of the numerical model, an initial limited parametric study has been carried out. This has led to improved guidelines for determining the geometry and density of core inserts in the design of sandwich X-joints exposed to compressive loading.

The achieved design guidelines for the compressive load case presented here will be combined with results from the damage tolerance investigations in part II [1].

2 Specimen configurations

An important design aspect is to ensure that the core inside the deck panel has sufficient strength, and for this purpose it is common to use a higher density piece of core in the region of the joint than is used in the remainder of the panel. The optimal size of the core insert is governed by the distribution of core stresses in the compression and tensile load cases. Furthermore, from a damage tolerance point of view it could also depend on the extent of steady-state fiber bridging in the tension load case in the presence of a debond at the interface between laminate and core, which will be considered in [1].

Two typically applied GFRP / PVC foam core X-joint configurations in naval ships have been chosen, see Fig. 1, with different fillet radii at the joint, see Fig. 2. The fillet radius (and thus the radius of the overlamination at the joint) has earlier been proven to be an important design parameter [2], and is believed to be governing for the shape and extent of the compressive and tensile stress distributions in the core. Wooden inserts, see Fig. 1, have been used to reinforce the core at all loaded and free ends of the specimens. These reinforcements will ensure that no local unwanted deformations occur at the clamped boundaries. Five specimens of each type have been manufactured and tested.

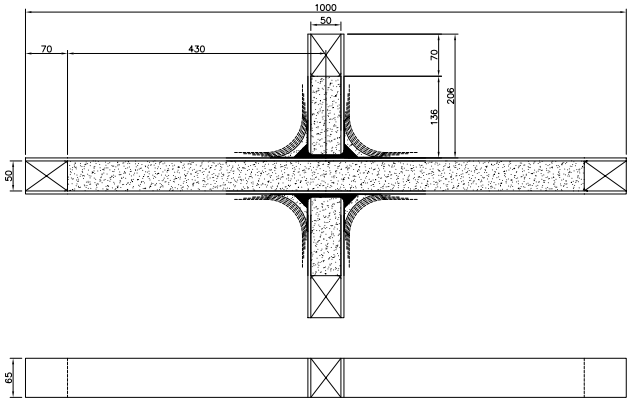

Fig. 1. Test specimen geometries. Shown for type X2, but type X1 has similar dimensions.

In both X-joint specimen types, the face laminates each consist of four quadri-axial, E-glass mats (Devold AMT DBLT-850, 850 g/m^2) with lay-up configuration $(0/45/90/-45)_{2s}$, together with polyester resin (Polylite 720-691), manufactured using vacuum assisted resin injection moulding. The resulting face thickness is approximately 3 mm.

The core is a 50 mm thick cross-linked PVC foam of the relatively heavy Divinycell H200 type, with a density of approximately 200 kg/m^3. The filler Norpol FI 177-10 has been applied in all joints. The two different design case specimens, X1 and X2, are similar in overall geometry but differ in terms of fillet geometry and overlamination techniques, see Fig. 2.

For the X1-type specimens the fillet radius is 25 mm and the overlaminations are made using E-glass fiber mats corresponding to the lay-up in the face laminates. The overlamination mats have a length of 150 mm and are placed staggered 16 mm in each layer relative to one another, as indicated in Fig. 2.

Apart from filler and overlaminations, the X2-type specimens also have a specially designed Divinycell H250 foam insert embedded in the filler material, thus increasing the fillet radius to 60 mm and reducing the weight. The fiber mats (same as for the X1 type) used for the overlaminations are of different length, increasing with 30 mm between each layer, i.e. four layers in all, in order to resemble the face laminate lay-up of the faces. The mats are placed symmetrically around the angle bisector of the fillet radius.

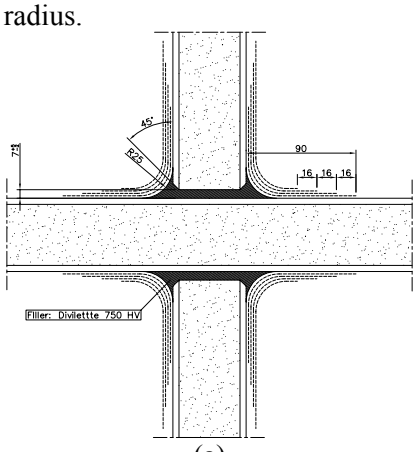

(a)

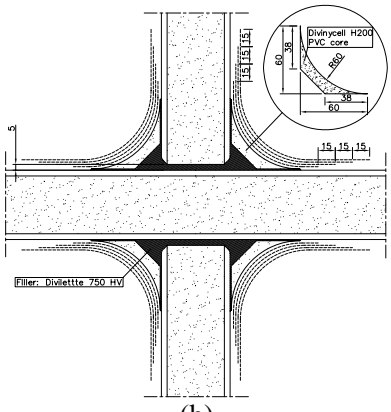

(b)

Fig. 2. Schematic representation of fillet and overlamination details. (a) Type X1. (b) Type X2.

3 Experimental set-up

A test rig, earlier used [5] for tests similar to those presented in part II [1], has been modified to accommodate the above described X-joints. In Fig. 3 the entire test rig is shown with an X-joint specimen installed.

The test rig is designed to simulate as closely as possible the actual boundary conditions for a deck/superstructure/bulkhead X-joint. The clamping of the two ends of the horizontal panel, which represent the through going deck panel, should be equivalent to the rigidity from the surrounding deck panel. However, the stiffness of the surrounding deck panel in the actual structure is highly dependent on the distance to the next bulkhead or stiffener. For simplicity the clamps are therefore chosen to be as rigid as possible, i.e. fully clamped allowing no displacements or rotations. The lower and upper ends (vertically aligned) should simulate the bulkhead and superstructure panels joined to the deck panel. Both of these are, similarly to the deck panel, cut-offs from larger panels and basically designed in the same way as the horizontal clamps, thus can be treated as fully clamped. These vertical joints help to keep the specimen aligned during testing, and reduce the column length of the panels, eliminating the risk of column buckling in compression.

The test rig is mounted in an Instron 8502 servo-hydraulic test machine. Compression loads are introduced into the specimens at a displacement-controlled loading rate of 1.5 mm/min, and measured by a 100 kN load cell. Full-field displacements and surface strains are measured at one side of the specimen using an advanced digital optical system (ARAMIS 4M) operating at a frequency of 0.25 Hz, see Fig. 4.

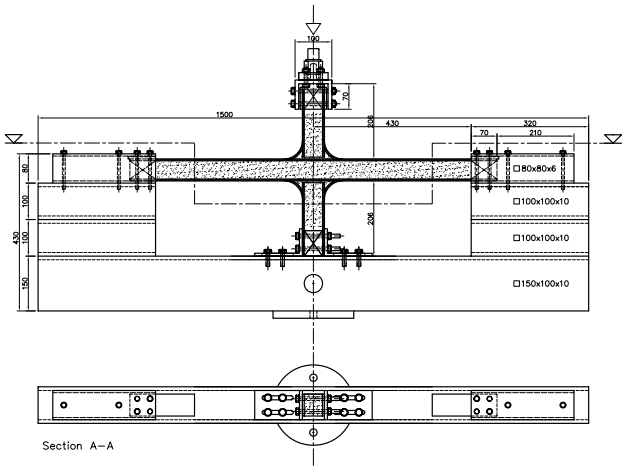

Fig. 3. Modified compression X-joint test rig

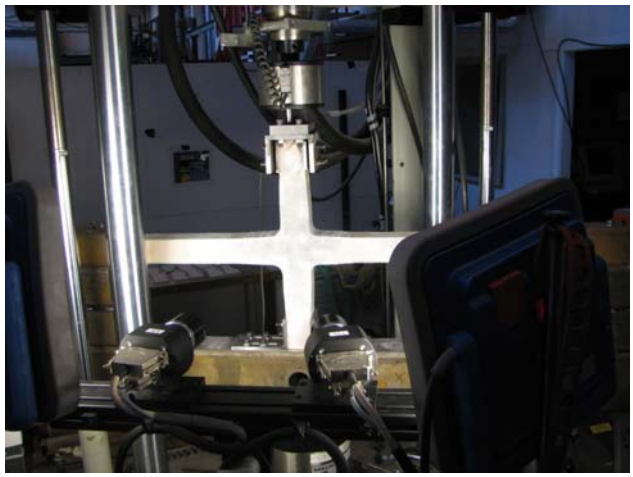

Fig. 4. Test rig with an X1 specimen and digital cameras.

4 Numerical models

All FE-modeling is done using the commercial FE code ABAQUS version 6.5, and the material models applied are all defined within this software.

Both 2D plane and 3D solid models have been developed. The mesh can be seen in Fig. 5. Related to the use of the Crushable Foam material model for the foam materials, linear plane and solid elements have been used. For the X1 specimens a total of 6169 quadrilateral CPE4R and triangular CPE3 plane strain elements have been used for the 2D model, and 9037 primarily hexahedral C3D8R solid elements for the 3D model.

For the X2 specimens 7838 primarily quadrilateral plane strain elements are applied for the 2D model. No solid model has been generated for the X2 case.. The minimum element size is 2 mm for the 2D models, see Fig. 6. Mesh convergence analyses have furthermore been carried out for all FE-models.

Implicit transient analysis is carried out using an unsymmetric storage matrix solver due to the Crushable Foam material model. In order to improve solution convergence, an artificially increased damping factor has been applied in the analyses. It has furthermore been shown that the artificial damping factor has negligible influence on the primarily static solution.

The compression force is applied as a nodal displacement boundary condition at a node created on top of the upper vertical hard-wood insert. This node is created by adding a triangle of very stiff material on top of the wooden insert, see Fig. 5.

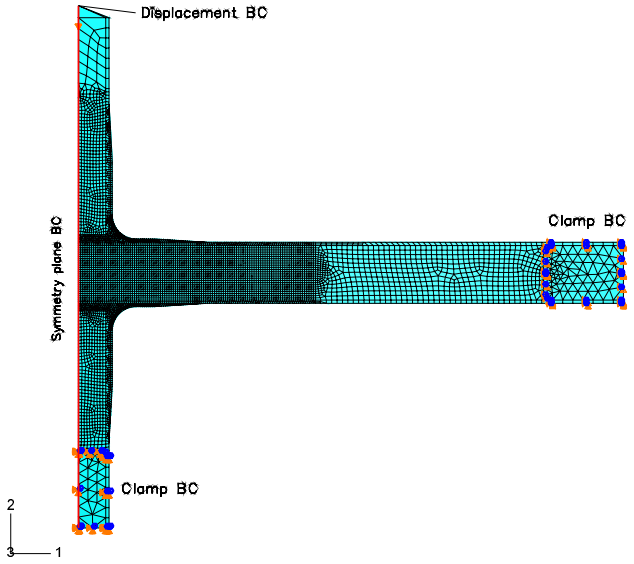

(a)

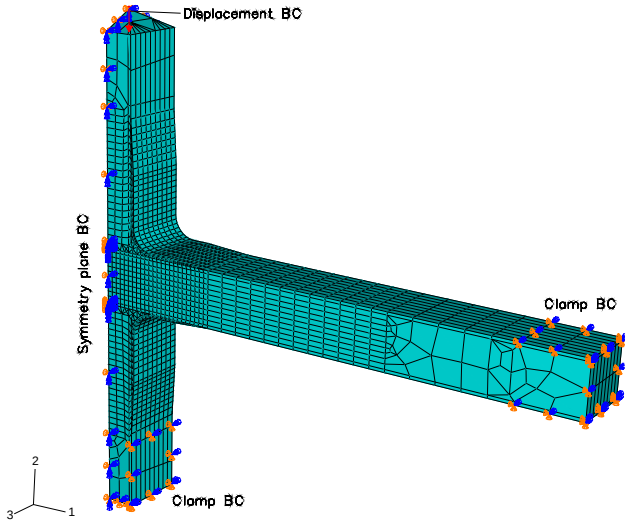

(b)

Fig. 5. 2D (a) and 3D (b) FE-model of the X1-specimen showing applied mesh, boundary and symmetry conditions.

To model the inelastic crushing regime and densification regime of the H200 and H250 PVC foam core materials, the Crushable Foam material model in ABAQUS is applied. The applicability of this material model is validated through simple FE-models compared with experimental tests on material specimens, but details concerning this study are beyond the scope of this paper. However, extensive material tests have been carried out to establish the input parameters for the Crushable Foam material model in ABAQUS, and they are given in Table 1. The density, and thereby the mechanical properties, vary significantly between the H200 foam sheets applied in both the material tests (odd H200) and the X-joint specimens. To allow for this the properties are scaled linearly with the density [6]. The elastic properties for the H250 foam type are based on datasheet values [6] and the in-elastic properties are scaled results from the H200 material tests.

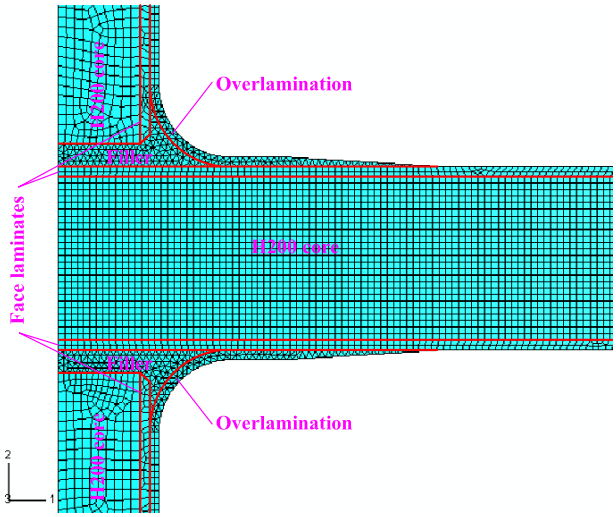

(a)

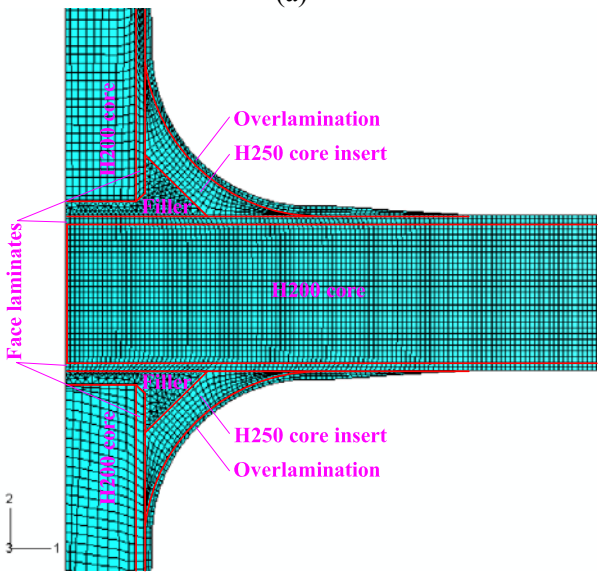

(b)

Fig. 6. Detailed meshing at the intersection for the X1 (a) and X2 (b) 2D FE-models.

The face laminates and overlaminations are modeled using a linear-elastic, orthotropic material model. In-plane material parameters (E-moduli and Poisson's ratio) have been measured in tensile tests. The remaining in-plane and out-of-plane properties have been estimated based on resin properties and an assumption of quasi-isotropic material behavior for the quadri-axial laminates. The applied material properties can be seen in Table 2.

Table 1. Input for the Crushable Foam material model; Young's modulus = E, Poisson's ratio = ν, ultimate stress (elastic) = $\sigma_{c,elastic}$ and ultimate strain (elastic) = $\varepsilon_{c,\,elastic}$. The logarithmic true stress, σ_t and the volumetric logarithmic strain, ε_v indicates characteristic points on stress-strain curves.

	Material tests (Odd H200)	X1 specimens	X2 specimens	H250
Density	240 kg/m^3	213 kg/m^3	238 kg/m^3	250 kg/m^3
E	250 MPa	222 MPa	248 MPa	300 MPa
ν	0.32	0.32	0.32	0.32
$\sigma_{c,elastic}$	5.2 MPa	4.6 MPa	5.1 MPa	6.2 MPa
$\varepsilon_{c,elastic}$	2 %	2 %	2 %	2 %
$\sigma_{t,1}$	5.3 MPa	4.7 MPa	5.3 MPa	6.3 MPa
$\sigma_{t,2}$	10.0 MPa	8.4 MPa	9.8 MPa	11.7 MPa
$\sigma_{t,3}$	63.7 MPa	53.7 MPa	62.8 MPa	74.0 MPa
$\varepsilon_{v,1}$	0 %	0 %	0 %	0 %
$\varepsilon_{v,2}$	42 %	39 %	42 %	43 %
$\varepsilon_{v,3}$	46 %	42 %	45 %	47 %

Table 2. Mechanical properties for face laminates and overlaminations.

E_1	E_2	E_3	ν_{12}	ν_{13}	ν_{23}
14.50 GPa	14.50 GPa	3.65 GPa	0.33	0.33	0.33
G_{12}		G_{13}		G_{23}	
5.45 GPa		1.37 GPa		1.37 GPa	

The Reichhold NORPOL FI-177 adhesive filler and the hard-wood insert material are both modeled as isotropic, linear-elastic materials. The compressive stresses in the adhesive filler do not reach the plastic yield limit during the analysis, thus the plastic regime is neglected. The applied material parameters can be seen in Table 3.

Table 3. Mechanical properties for the adhesive filler and beech-wood core inserts [7].

Adhesive filler		Beach wood	
E	ν	E	ν
289 MPa	0.30	13.13 GPa	0.30

5 Comparison of experimental and numerical results

5.1 Overall structural behavior

In Fig. 7 the compressive load divided by the specimen width is shown as a function of the piston displacement. Here the first linear relationship corresponds to elastic deformation of the foam core in the horizontal panel, possibly including smaller settlements of the test setup especially for the X1 specimens. The slopes for the two types, X1 and X2, are seen to be almost identical. Based on both experimental and numerical results, the load levels at which the response softens, i.e. the foam starts crushing, are approximately 650 kN/m for type X1 and 900 kN/m for type X2. It can be concluded that the major and obvious difference between the two joints is the difference in the radii of the overlaminations and thereby the ability to distribute the strains evenly. When the foam material begins crushing, aspects related to the material non-linearity begin to influence such aspects as how the stiffer elements interact. This interaction between the laminates, fillets and fillet inserts causes the specimens to fail at different stages.

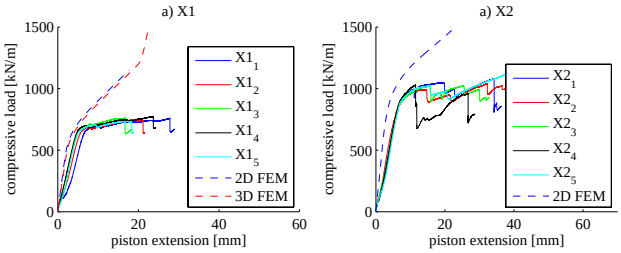

Fig. 7. Compressive load per unit width as a function of the applied vertical displacement for specimens X1 (a) and X2 (b).

Comparing experimental and numerical results, the FE models follow reasonably well the global response from the experimental tests in the initial, linear load-displacement range. The transition point where the slope of the response changes is considered as the failure load for design purposes. The load magnitudes at this point agree well between numerical and experimental results for both X1 and X2 specimens, with deviations around 8%. The deviations in the whole linear response regime can probably be attributed to the varying core density and mechanical properties not only between the individual specimens, but also through the thickness of the core sheets. Furthermore, the adhesion between the different structural components is not taken into account in the FE models, and lack of rigidity of the test fittings could also have an influence on the stiffness, especially the upper clamp at which the displacement is applied.

The significant differences in the slopes beyond the initial failure load point for the experimental and numerical load-displacement plots in Fig.7 are related to the FE modeling restrictions set by the Crushable Foam material model. Only plane strain elements are applicable for this material model, preventing the significant out-of-plane

strains that are observed in the experiments, see Fig. 12. The stiffer response of the plane strain FE model could also be related to the deviations seen in the linear regime as discussed above.

Applying the 3D FE-model showed that modeling the X-joint using 3D solid elements, in order to take the specimen width into account, did not improve the correlation with experimental results, see Fig. 7. However, the plane strain Crushable Foam material model was also applied in the 3D model which most likely is the cause of the continued deviation. This leads to the conclusion that a more suitable 3D material model for the H200 core material should be applied in the 3D model or a similar material model in plane stress should be applied in the 2D model. Development of a new material model is out of the scope for this paper, but should be considered in future work.

However, it could be argued that the plane strain FE results actually simulate the behavior realistically for an X-joint integrated in a larger structure where the surrounding structure would create a strain restriction out-of-plane more equal to a plane strain situation.

5.2 Surface strain measurements and failure

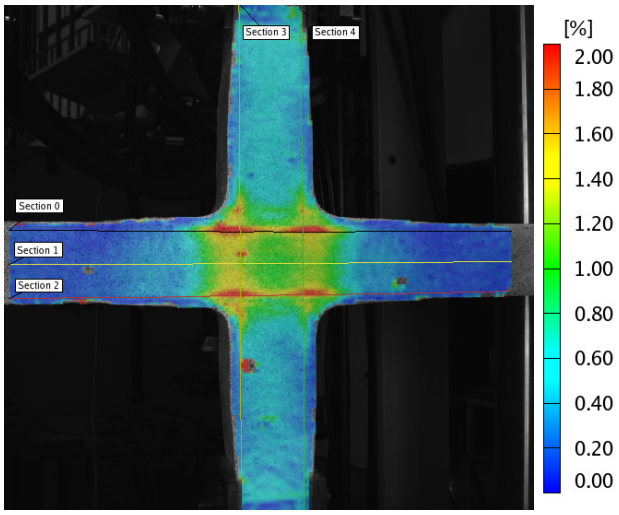

Fig. 8. Location of sections used for data extraction and von Mises strain overlay plot at approx. 461 kN/m. Specimen $X1_3$.

In the digital optical system (ARAMIS 4M), displacement and strain data are extracted both through contour plots and using manually defined sections. These sections are represented by points along a path. Three horizontal sections in the horizontal core panel are defined for all specimens. Sections 0 and 2 are located 2 mm from respectively the upper and lower face/core interfaces in the core, and section 1 is located in the middle of the core. Two vertical sections (3 and 4) are located 2 mm from the face/core interfaces of the vertical core panel going all the way through the joint. All sections can be seen in Fig. 8.

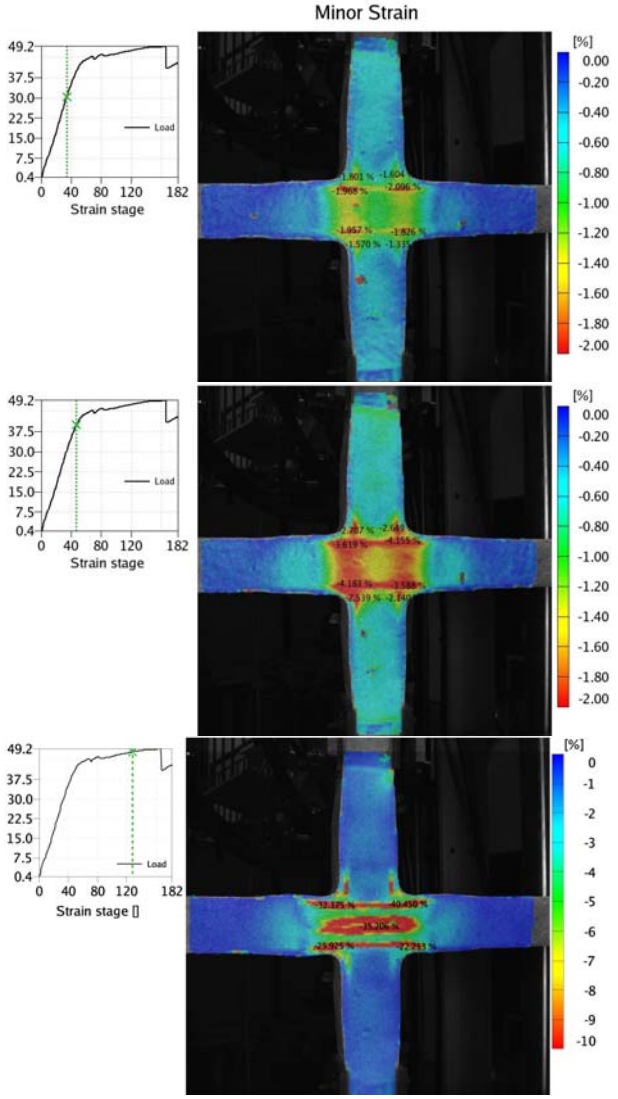

Fig. 9. Minor strain distributions at representable load levels for specimen $X1_3$.

Fig. 9 shows the minimum principal strain, i.e. the maximum principle compressive strain (from hereon referred to as “minor strain”) overlay for specimen $X1_3$ at three different strain stages, which, as the left graphs indicate, corresponds to load levels at significant behavioral points. Notice that the load is not divided by the specimen width and therefore only the behavioral progress can be compared to the results of Fig. 7. Fig. 9 also illustrates the double symmetry appearing in the X-joint. From this strain plot, the location of hard spots can be identified as

being in the core near both face/core interfaces in the horizontal panel, but inside the core.

In the first plot in Fig. 9 the load has reached 460 kN/m (30 kN on the graph), and strain values have reached the crushing limit of 2% at the first initiation points. At the next plot in Fig. 9, the load has reached 615 kN/m (40 kN). The crushing strain values have at this stage developed all the way through the core thickness, and as shown in the graph, it is just prior to the loading capacity (break-off) point and thereby the crushing regime of the foam material. The last plot in Fig. 9 shows severe deformation in the joint, at a load level of approximately 730 kN/m (47 kN). This load level is well above the critical crushing regime of the foam and at this point very large global displacements are taking place throughout the joint, see also Fig. 12. At this stage the stiffer components in the joint are exposed to damaging strains, and interaction between these stiffer elements will eventually lead to failure. The detailed analysis of the actual failure mechanism will be left out here, but the final failure is a shear/ delamination failure between the overlaminations and horizontal face laminates, as shown in Fig. 10.

In Fig. 7 it was shown that the X2 specimens correlated very well in the linear elastic regime, but beyond the loading capacity point, they behaved slightly less consistently compared to the X1 type results. This should be kept in mind during the following explanation of the structural behavior of the X2 specimens.

Fig. 10. Final failure of specimen $X1_1$.

Fig. 11 shows the minor strain overlay for specimen $X2_5$ at four different strain stages at significant behavioral load points. The first plot in Fig. 11 shows that, for the X2-type, vertical symmetry is present but the symmetry about the horizontal centre-line is less pronounced. As with the X1-type the strains reach the crushing value of 2% at the interface in the horizontal sandwich panel. In contrast to the X1-type, however, the crushing strains initiate at the lower interface and not at both interfaces, indicating that there is a difference between the strains at the upper and lower interfaces. This difference is due to the membrane effect introduced by the vertical translation restriction on the horizontally clamped ends combined with a sole movement of the upper vertical panel while keeping the lower panel fastened. The most severe strains occur, as with the X1-type, in the more ductile foam material. The exact deterioration of the load carrying capacity is described in the following.

In the first plot in Fig. 11 the load has reached 615 kN/m (40 kN), and strain values have reached the crushing limit of 2% at the first initiation points. At the next plot in Fig. 11, the load has reached a level of 770 kN/m (50 kN). The red areas, corresponding to crushing strain values, have at this stage developed nearly all the way through the core thickness, and as shown in the graph, the plot is taken from the moment just prior to the loading capacity point and thus the crushing regime of the foam material. The third plot in Fig. 11 shows severe deformation at a load of approximately 1015 kN/m (66 kN). This load level is just above the critical crushing regime (break-off point) of the foam, but before the two smaller load drops. At this point large global displacements start to take place throughout the joint. These large displacements initiate failure in the two upper overlaminations, see Fig. 12. The last plot in Fig. 11 shows the deformation at a load of approximately 1090 kN/m (71 kN). In this plot the two failures in the overlaminations can again be seen together with large deformation of the core material in the horizontal panel, just before subsequent failure by overlamination separation from the face of the horizontal panel.

In Fig. 12 it can be seen that foam crushing takes place in the middle of the foam core in a horizontally extended region corresponding approximately to the width of the overlaminations. The extent of this crushing region differs from that for the X1-type and this is the primary reason why the X2-type can withstand more loading before break-off (foam crushing) takes place. Furthermore, when comparing the failure of the two X-joint types, it is seen that the X2-type indents into the relatively soft foam insert directly underneath the laminate, whereas in the X1 type, the overlamination is supported by the somewhat harder filler material and indentation is not possible. Fig. 12 shows how the overlaminations fail in the X2 joint, which correlates to the behavior seen in Fig. 7 and 11, where two smaller load drops, of approximately 50-100 kN/m occur after a regime of foam crushing. These two smaller load drops, which originate from each of the

two overlamination failures, are seen to be of approximately the same size for each of the specimens.

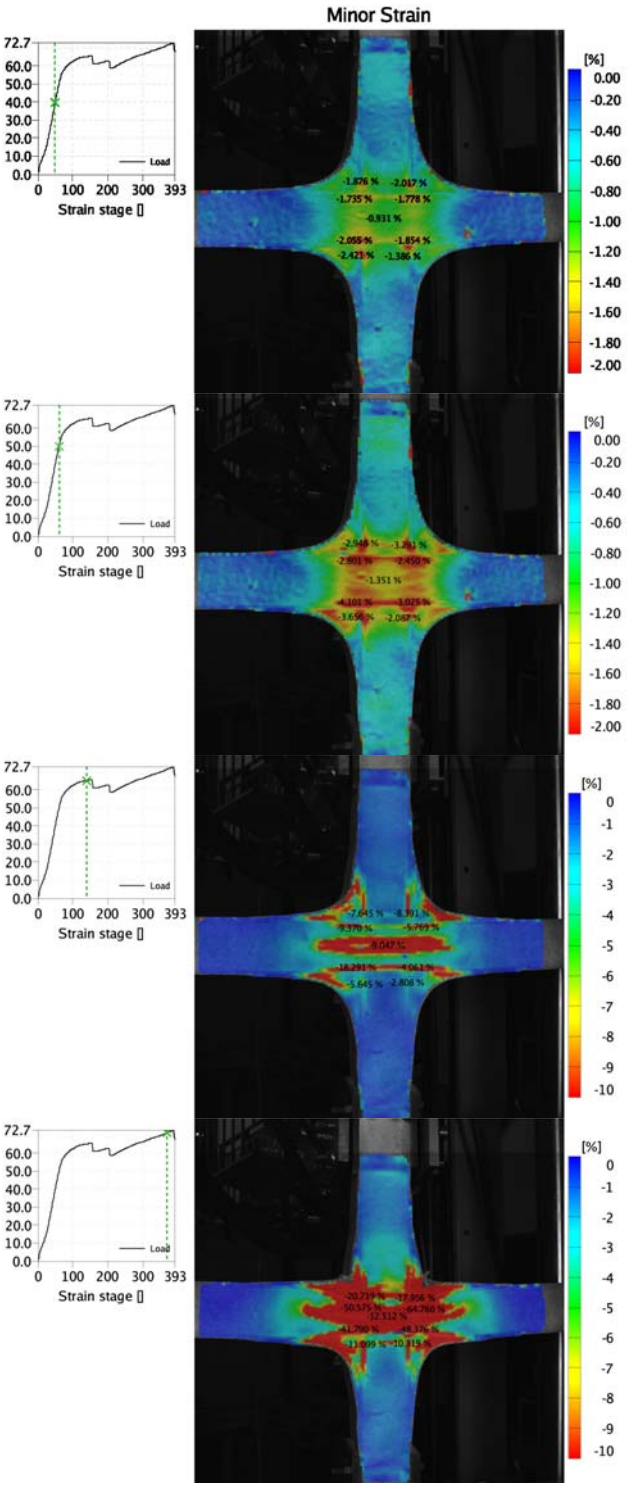

Fig. 11. Minor strain distributions at four load levels for specimen $X2_5$.

These final failures of the X2-type differ somewhat and are generally seen to be less consistent than those of the X1 type.

Fig. 12. Large deformations in the core and failure of upper overlaminations in the $X2_1$ specimen.

5.3 Strain analysis and comparison

In Fig. 13(a), (b) and (c) the minor strains at the three horizontal sections defined in the horizontal panel, see Fig. 8, are plotted at load levels within the linear regime (approx. 300-330 kN/m) for the X1-type specimens. For plots (a) and (c) the strain distributions and magnitudes from the FE models are very similar to the experimentally obtained results. For the section 1 plot, defined in the mid-plane of the core, the FE results slightly exaggerate the strain magnitudes. This is probably related to the variations in density through the thickness of the core, which are ignored in the FE model. The negative peaks on the (a), (b) and (c) plots originate from the high stresses distributed from the stiff vertical face laminates through the filler and the horizontal face laminate into the flexible H200 core.

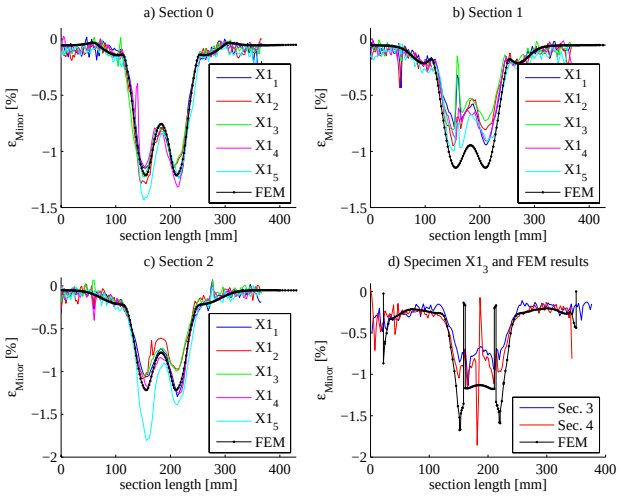

Fig. 13. Minor strain section plots for the X1-joints. Exact compressive loads: $X1_1$ = 310 kN/m, $X1_2$ = 308 kN/m, $X1_3$ = 318 kN/m, $X1_4$ = 315 kN/m, $X1_5$ = 315 kN/m, 2D FEM = 333 kN/m.

Plot (d) in Fig. 13 presents the strains at the two vertical sections from the experimental tests with specimen $X1_3$ together with the corresponding results from the 2D FE model. The strain peaks at the ends of the plots originate from the singularities connected with the load transfer between the stiff hard-wood inserts and the relatively soft core. The extreme deviations in the middle of section 4 from the experimental tests should be ignored and are related to single, excessively distorted facets in the digital optical system. As seen for the horizontal sections, the two negative peaks represent the strain concentrations related to the stress transfer from the stiffer vertical face laminates to the core. The two positive peaks, most pronounced in the numerical results, represent the bending strains in the stiff horizontal face laminates. Generally the strain concentrations are more pronounced in the numerical results, since the element size in this model gives a higher resolution than the facet size used for the strain pictures recorded by the digital optical system.

Regarding the design of core inserts for the horizontal core panel, the horizontal extent of the strains is important in order to determine a required insert length. It is seen in Fig. 13(a), (b) and (c) that this extent is well simulated by the numerical model, and in particular the correlation is excellent towards the outer ends of strain field.

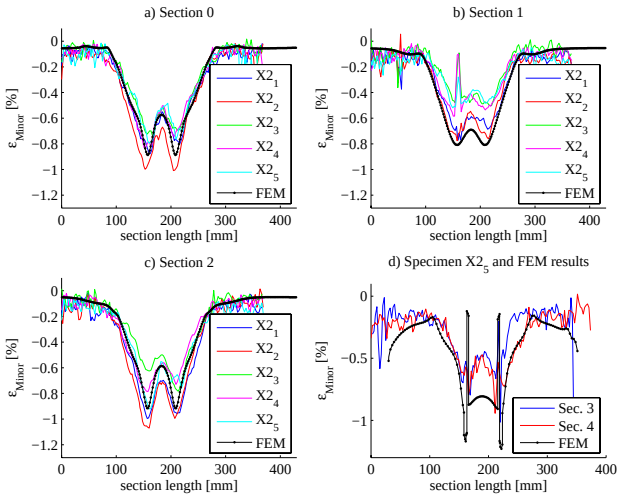

Fig. 14. Minor strain section plots for the X2-joint. Exact compressive loads: $X2_1$ = 317 kN/m, $X2_2$ = 367 kN/m, $X2_3$ = 311 kN/m, $X2_4$ = 329 kN/m, $X2_5$ = 314 kN/m, 2D FEM = 320 kN/m.

The minor strains along the horizontal sections in Fig. 14(a), (b) and (c) for the X2-specimens for loadings within the linear regime of approximately 310-370 kN/m show again excellent agreement between the experimental and numerical results. However, as seen for the X1-joint, the numerical section 1 plot reveals a slight overestimate of the strains. This is again related to the non-homogeneous core being modeled as homogeneous with isotropic properties. The vertical sections in Fig. 14(d) display the same characteristics as for the X1-case; the numerical model predicts the strain peaks better as a consequence of the higher resolution, i.e. element size vs. facet size.

The overall strain distributions for the numerical model are hereby considered validated by the experimental results within the linear regime. A similar comparison in the crushing regime, i.e. beyond the loading capacity point, is not carried out here, as this loading regime is not relevant for the determination of the core insert length.

6 Improved design guidance

A core insert works as a reinforcement of the horizontal core panel, in order to prevent or delay the local failure of the core by, for example, crushing under compressive loading, which is seen to lead to subsequent failures as described above. The schematic layout of a core insert in an X-joint is presented in Fig. 15.

If it is assumed that, in order to maintain structural integrity, the core must not undergo crushing, the insert length is determined by the extent of the core which experiences minor strains greater than the compressive ultimate strain for the H200 core material (see Table 1) of 2% for a given load level.

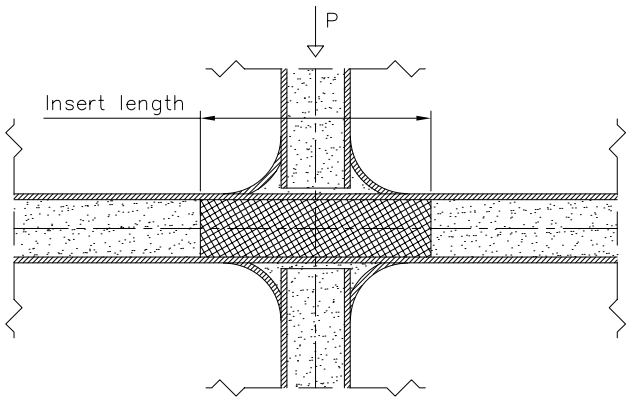

Fig. 15. Schematic layout of core insert in X-joint and core insert length definition.

Fig. 16 visualizes the core insert analysis and validates the numerical results within the tested load regimes, making the FE models suitable as design tools for core inserts. Furthermore, it is fair to assume that an insert length of 200 mm is more than

sufficient in order to withstand loading in the crushing regime, as the agreement between numerical and experimental results was good in the outer ends of the strain field even for high crushing loads (not shown in detail in this paper). However, for the X1-joint the required insert length should be approximately 110 mm and for the X2-joint the length should be approximately 130 mm, in order to withstand the compressive forces up to the defined design loading capacity set by the crushing regime of the H200 core, 600 kN/m and 900 kN/m for the X1 and X2-joints respectively.

The results indicated in Fig. 16 are only valid for the two studied X-joint geometries and with the chosen materials. However, similar design curves can readily be developed for other design cases.

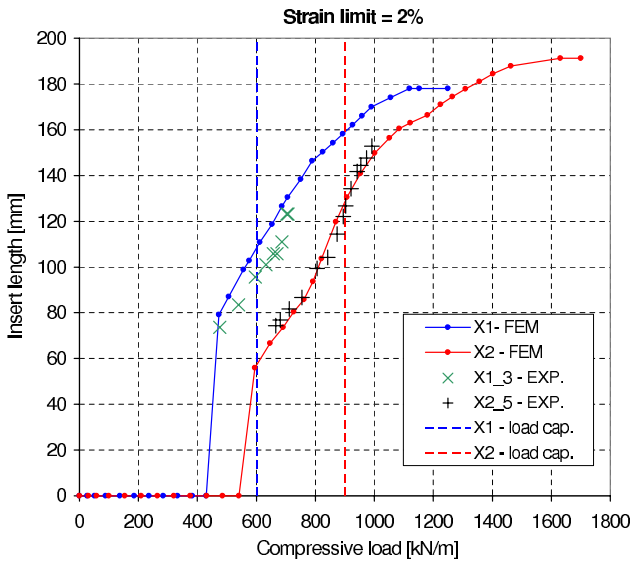

Fig. 16. Required core insert length as a function of the applied compressive load for which the joint is designed.

In the above approach the actual maximum capacity of the joint will depend on the chosen insert material replacing the H200. An alternative approach could be to consider that H200 is the chosen insert material and that the compressive strain in this material should not exceed the 2% crushing initiation value. This approach would readily give the maximum capacity of the X-joint, and the required insert length could then be determined by assuming a lower bound value (e.g. 0.2 %) for the maximum strain allowed in the lower-density core material adjacent to the insert.

7 Conclusion

Two alternative designs of sandwich X-joints have been studied for the case of compressive loading. Results from laboratory tests and FE simulations using a crushable foam model for the core agree quite well in terms of load-displacement curves and strain distributions. However, in the core crushing regime the FE analysis predicts a significantly stiffer behaviour than seen in the tests. This is probably caused by restriction of deformations to plane strain in the core material model, which is probably more representative of a practical application than the free out-of-plane deformation allowed by the rather narrow test specimens.

For the case of Divinycell H200 PVC foam core, design curves have been derived that show the extent of the region in the core of the through-going sandwich panel that will experience crushing at a given load level for each type of X-joint, and which needs to be replaced by a block of higher-strength material. Similar curves can readily be developed for alternative X-joint designs and foam cores.

8 Acknowledgements

This work has been performed within the context of the Network of Excellence on Marine Structures (MARSTRUCT) partially funded by the European Union through the Growth Programme under contract TNE3-CT-2003-506141. The provision of all the test specimens by Kockums AB (Karlskronavarvet) is highly appreciated.

References

[1] Lundsgaard-Larsen, C., Berggreen, C., Karlsen, K., Jenstrup, C. and Hayman, B., "Improving performance of polymer fiber reinforced sandwich X-joints in naval vessels – Part II: Damage Tolerance". *16th International Conference on Composite Materials*, Kyoto, Japan, 2007.

[2] Kildegaard, C., "Experimental and numerical fracture mechanical nmstudies of FRP-sandwich T-joints in maritime constructions". *2nd Int. Conference on Sandwich Constructions*, Gainesville, USA, 1992.

[3] Efstathios, E. and Moan, T., "Experimental and numerical study of composite T-joints". *Journal of Composite Materials*, Vol. 30, No. 2, 190-209, 1996.

[4] Toftegaard, H. and Lystrup, A., "Design and test of lightweight sandwich T-joint for naval ships". *Composites: Part A*, Vol. 36, No. 8,1055-1065, 2005.

[5] Berggreen, C., Simonsen, B.C. and Borum, K.K., "Experimental and numerical study of interface crack propagation in foam-cored sandwich beams". *Journal of Composite Materials*, 41(4):493-520, 2007.

[6] http://www.diabgroup.com/europe/literature/e_pdf_files/man_pdf/H_man.pdf

[7] http://www.matweb.com/search/SpecificMaterial.asp?bassnum=PTSE030